University of Glasgow

Prasojo, O. A., Hoey, T. B., Owen, A. and Williams, R. D. (2022) Slope break and avulsion locations scale consistently in global deltas. *Geophysical Research Letters*, 49(2), e2021GL093656.

(doi: 10.1029/2021GL093656)

The material cannot be used for any other purpose without further permission of the publisher and is for private use only.

There may be differences between this version and the published version. You are advised to consult the publisher's version if you wish to cite from it.

This is the peer reviewed version of the following article:

Prasojo, O. A., Hoey, T. B., Owen, A. and Williams, R. D. (2022) Slope break and avulsion locations scale consistently in global deltas. *Geophysical Research Letters*, 49(2), e2021GL093656, which has been published in final form at: 10.1029/2021GL093656

This article may be used for non-commercial purposes in accordance with Wiley Terms and Conditions for Self-Archiving.

https://eprints.gla.ac.uk/261990/

Deposited on: 6 January 2022

Enlighten – Research publications by members of the University of Glasgow
http://eprints.gla.ac.uk

Check for updates

Accepted Article

Slope break and avulsion locations scale consistently in global deltas

O. A. Prasojo[1,2*], T. B. Hoey[3], A. Owen[1] and R. D. Williams[1]

[1] School of Geographical and Earth Sciences, University of Glasgow, University Avenue, Glasgow, G12 8NN, United Kingdom.

[2] Geoscience Study Program, Faculty of Mathematics and Natural Sciences, Universitas Indonesia, Depok 16424, Indonesia.

[3]Department of Civil and Environmental Engineering, Brunel University London, Uxbridge, UB8 3PH, United Kingdom.

Corresponding author: Octria Adi Prasojo (o.prasojo.1@research.gla.ac.uk)

Key Points:

- Morphometric boundaries investigated in 105 modern deltas globally
- Slope break and avulsion lengths show the strongest scaling relationship, more significant than previous scaling relationships
- Processes contributing to this slope-break avulsion length scaling relationship are proposed along with conceptual model of the implications

This article has been accepted for publication and undergone full peer review but has not been through the copyediting, typesetting, pagination and proofreading process, which may lead to differences between this version and the Version of Record. Please cite this article as doi: 10.1029/2021GL093656.

This article is protected by copyright. All rights reserved.

Abstract

Understanding how deltas respond to changing sea level is crucial as deltas provide important ecosystems, are inhabited by ~500 million people, and are nexuses of food, energy and economic activity. The response of delta distributary channels to sea-level rise depends on the geomorphic controls on delta morphology and their scaling relationships. Our data from 105 deltas globally show strong scaling between the upstream distances to slope breaks and to avulsion nodes, and confirm the previously-known scaling between backwater and avulsion lengths. The break in slope is proposed to be the principal control on delta development, along with other proposed secondary controls. We identify and discuss the implications of this slope break-avulsion length scaling, leading to a conceptual model of delta morphology and sedimentology. This model suggests how deltas may respond to future sea level rise and guides interpretation of deltaic deposits in the rock record.

Plain Language Summary

River deltas across the globe are being affected by sea-level rise. How deltas respond to this rise is thought to be related to a region (known as the backwater zone) where the river flow velocity starts to decrease due to river slope reducing as the flow approaches the sea. The location of this zone has been shown to scale with the location of abrupt shifts (known as avulsions) in the position of delta channels. However, we do not have a complete understanding of why and where these shifts occur. By analyzing 105 river deltas globally, we found that the strongest scaling relationship is between the distances from the shoreline of avulsion and of a change in slope. Due to this strong scaling relationship, we propose that river deltas may respond to sea-level rise differently depending on their shape and gradient, and the location of the slope change on the delta itself.

1 Introduction

Deltas, alluvial protrusions beyond lacustrine or marine shorelines, are one of Earth's essential landscape types and provide a wide range of ecosystem services (Besset et al., 2017); ~500 million people currently live on deltas which have been important locations in the development of human societies and are significant centers for biodiversity (Ericson et al., 2006; Nienhuis et al., 2020; Syvitski & Saito, 2007). However, deltas are particularly vulnerable to a combination of changing sea-levels, reduced sediment influx and subsidence, causing increasing flood risk and degradation of ecosystems (Besset et al., 2019; Hoitink et al., 2017; Mueller et al., 2017; Syvitski et al., 2009; Tessler et al., 2015; Wang et al., 2017; Warrick et al., 2019; Wu et al., 2020; Yang, 2005).

When a sediment-conveying river enters a water body, delta lobes start to develop from mouth bar deposition, forming a delta planform with distributary channel networks. Excepting many lake deltas, most open water deltas are exposed to marine energy in the form of tides, waves, and storm surges and are also affected by relative sea-level rise (Hoitink et al., 2017). The complexity of distributary channel networks depends on interactions between factors including sediment supply, slope, climate, channel bifurcation and avulsion, with delta morphology reflecting the balance of these factors (Edmonds & Slingerland, 2008; Jerolmack & Mohrig, 2007; Syvitski et al., 2009). To understand how distributary channels will respond to rising sea level, the controls on the morphology of these channels need to be firstly understood.

This article is protected by copyright. All rights reserved.

Accepted Article

The presence of a body of water generates a distal backwater in delta channels, the length of which has been proposed as a fundamental hydrodynamic boundary in delta systems (Jerolmack & Swenson, 2007; Paola & Mohrig, 1996). This backwater zone is characterized by downstream decreases in grain size, channel migration rates and channel belt widths, and increased channel depth (Fernandes et al., 2016). A study of nine modern deltas showed that the backwater length (L_b) scales with the avulsion length (L_a), which is the distance from the shoreline to the first (i.e. farthest upstream) bifurcation along the river centerline (L_a:L_b ~1:1 to 1:2) (Chatanantavet et al., 2012; Ganti et al., 2016; Jerolmack & Swenson, 2007). This scaling relationship is considered crucial for defining the location of the preferential avulsion node and for understanding avulsion migration in the delta lobe building process (Brooke et al., 2020; Chadwick et al., 2019; Chatanantavet et al., 2012; Ganti et al., 2019; Nijhuis et al., 2015). However, Hartley et al. (2017), found a less consistent avulsion and backwater length scaling relationship from 13 modern deltas. Hartley et al. (2017) argued that an avulsion node, that they referred to as the delta apex, is primarily controlled by processes at the valley mouth where unconfined deposition commences. The position of the valley mouth coincides with the location of a longitudinal slope break that triggers the onset of delta construction in an unconfined setting, due to sediment transport capacity being reduced downstream from this location to the shoreline. Thus, there should be spatial correlation between valley mouth locations and avulsion node positions. However, valley mouth location is not necessarily the upstream limit of the coastal backwater. Hence, for deltas in equilibrium with external controls, Hartley et al.'s (2017) results suggest 1:1 scaling relationships between both the avulsion (L_a) and slope break (L_s) lengths measured from the shoreline and the valley-exit-to-shoreline distance (L_v).

The discrepancies between previous results, from small numbers of deltas, highlight the need to investigate generic scaling relationships on deltas using a larger data set. This study investigates morphometric boundaries (backwater, avulsion and slope break lengths, and valley-exit-to-shoreline distance) from a global data set of 105 modern deltas, considering the effects of landscape-scale (catchment size, river discharge, valley type) and local (water surface slope) factors. We also identify and discuss the processes contributing to these generic scaling relationships. Scaling relationships are fundamental to our understanding of delta development, allowing insights into how delta distributary channels will respond to changing allogenic and autogenic forcing.

2 Materials and Methods

A global dataset of 105 mostly river-dominated deltas that debouch into open seawater was analyzed (Fig. S1a & Table S1). We used Google Earth Engine (GEE) to compile 30 m resolution Landsat 5 tile images from 1984-2009, and digital elevation models (DEM) from the Shuttle Radar Topography Mission (SRTM) for 60°S to 60°N and ArcticDEM for north of 60°N (Farr et al., 2007; Morin et al., 2016; Tucker et al., 2004). We chose the least cloudy and oldest Landsat 5 images available from GEE to avoid engineered river banks that have become increasingly more prevalent (Fig. S2). SRTM and ArcticDEM resolutions are ~30 m and ~0.5 m, respectively. We used the DEMs to generate elevation profiles along the centerline of the main distributary channel in QGIS using the Terrain Profile™ tool. Only four deltas, all within ArcticDEM, show gross error that prevent extraction of a reliable elevation profile (Błaszczyk et al., 2019). We defined valley types through analysis of the topography using the method from Hartley et al. (2017). Catchment areas were obtained from the HydroBASINS level 6 global watershed dataset (Lehner & Grill, 2013). Since climate is a fundamental factor influencing delta

This article is protected by copyright. All rights reserved.

Accepted Article

morphology (e.g. river discharge, sea-level, wave action, storm energy, sediment yield), we classified deltas according to their dominant climate zone (Correggiari et al., 2005; Syvitski & Saito, 2007; Ta et al., 2002). Climate-based classification enables us to classify the data set more consistently across different delta morphologies (Table S1).

The satellite imagery analyzed here provides static snapshots of modern delta conditions. Dynamic environmental variables, including daily to annual tides and wave conditions, and decadal sea-level change and local subsidence are thus excluded. We manually identified each delta that has a subaerial deposit that protrudes beyond the lateral shoreline (Caldwell et al., 2019). Criteria for selection include any channel mouth that intersects with the open seawater depositing sediment that protrudes beyond the lateral shoreline, with or without the characteristic morphology of river-dominated deltas (e.g. subaerial mouth-bar deposit, elongate distributary channels) (Olariu & Bhattacharya, 2006). A sub-set of ten deltas, defined as wave-dominated by Nienhuis et al. (2020), are also investigated.

Avulsion length (L_a) was measured in ArcGIS along the river centerline from the shoreline at the time of the Landsat image to the first (farthest upstream) deltaic avulsion, hence assuming that this first avulsion is the delta apex node (Jerolmack & Swenson, 2007; Fig. S1b). Where there is a single active channel and no bifurcation, L_a was measured up to the farthest upstream valley exit point identified in the DEM, following Hartley et al. (2017). The slope break length (L_s) was defined from the elevation profile as the river distance between the shoreline and the first break in slope (Fig. S1c; Fig. S3; Fig. S4). Slope breaks were identified using a semi-automated local gradient method and Hack's Stream-Length (SL) index (Hayakawa & Oguchi, 2006; Supporting Information[1]). Valley-exit-to-shoreline distance (L_v) was measured along the river centerline from the shoreline to the valley exit point identified from the DEMs (Hartley et al., 2017).

Backwater length (L_b) was calculated (Chatanantavet et al., 2012) as:

$$L_b = \frac{h_c}{S} \quad (1)$$

and

$$h_c = \left(\frac{C_f {Q_c}^2}{g {W_{av}}^2 S}\right)^{\frac{1}{3}} \quad (2)$$

where h_c is the characteristic flow depth (m) and S is water surface slope (m/m) (Eq. 1). Characteristic flow depth (Eq. 2) was calculated using the bed friction coefficient C_f = 0.002 for large lowland rivers (Parker et al., 2007). Q_c is the characteristic water discharge (m^3/s), g is gravitational acceleration (m/s^2) and W_{av} is the channel width (m) at the avulsion node at the time of the image (Parker et al., 2007).

Characteristic water discharge (Q_c) is taken as the 2-year recurrence interval flood (Q_2) as close to the upstream limit of the delta as data availability allows, to provide an indicator of the dominant channel-forming flow (Ganti et al., 2016; Wolman & Miller, 1960). Q_2 was calculated from daily river discharge data available from the Global Runoff Data Centre (GRDC). For some deltas, only monthly river discharge data were available and Q_2 from these monthly data were converted to equivalent daily Q_2 values using empirical transformations for different climates (Fig. S5; Beck et al., 2018). Channel width (W_{av}) was measured on the Landsat imagery at the avulsion node to avoid influence by wave or tidal processes (Fig. S1b). Slope (S) was calculated from the water elevation profile along the centerline of each river.

This article is protected by copyright. All rights reserved.

3 Results

Measured (valley-exit-to-shoreline distance, avulsion and slope break lengths) and calculated backwater lengths are plotted in Figure 1. The L_a-L_b plot (Fig. 1a) shows a power-law relationship $L_a = 9.77L_b^{0.49}$ (R^2 = 36%; RMSE = 0.46). The equivalent L_s-L_v relationship is $L_s = 0.45L_v^{1.10}$ (R^2 = 46%; RMSE = 0.46) (Fig. 1b). Statistically, the most significant scaling is for the avulsion length against the slope break distance from the shoreline, with $L_a = 0.6L_s^{1.00}$ (R^2 = 63%; RMSE = 0.36) (Fig. 1c). Note that we show fewer than 105 deltas on Fig. 1 due to river discharge data being unavailable for some rivers, unidentified valley-exit points, and indeterminate slope breaks.

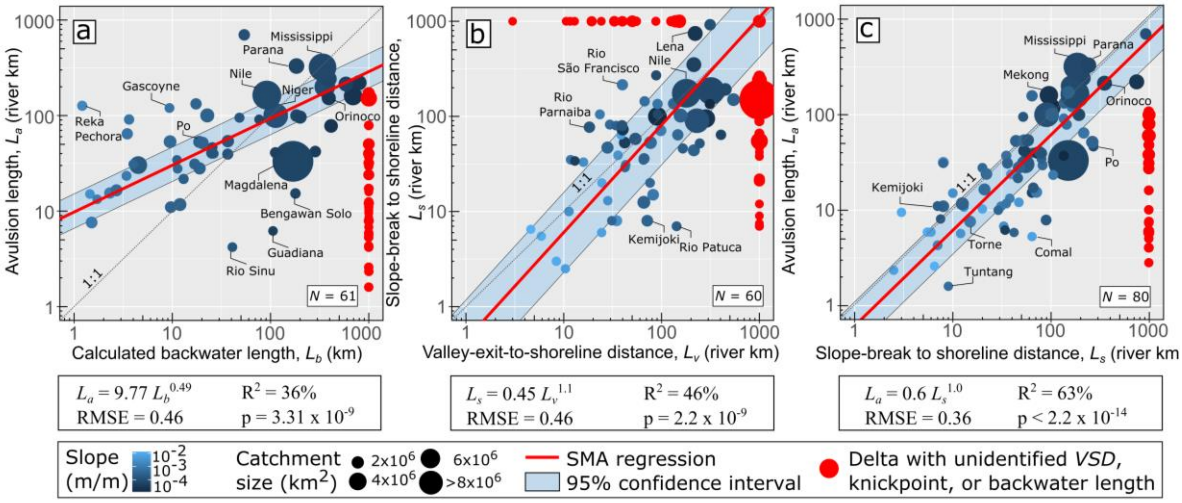

Figure 1. (a) Measured avulsion length (L_a) against calculated backwater length (L_b). (b) Slope break distance from the shoreline (L_s) against the valley-exit-to-shoreline distance (L_v). (c) Measured avulsion length (L_a) against the slope break distance from the shoreline (L_s). We used standard major axis (SMA) regression (red lines) to determine functional relationships. Point size is scaled with the catchment area; point color shade represents the slope of each delta. Root mean square error (RMSE) is in log units. Red points representing unidentified L_v, L_s and L_b are positioned on the border of the plots.

Decreases in water surface slope (blue points in Fig. 1 are shaded from dark to light as slope increases) are neither correlated with longer backwater, avulsion nor slope break lengths (Fig. 1a-c). Compared to the plot against the backwater length (Fig. 1a), larger catchment areas show a more significant correlation with slope breaks and avulsion lengths, consistent with prior literature (Fig. 1c; Fig. S6; Syvitski & Saito, 2007). The data contain some significant outliers, mainly from European sites, which are potentially affected by engineered river-banks (e.g. Guadiana, Po). Smaller deltas (L_a < 50 km; e.g. Tuntang, Comal) also contribute to these outliers. Therefore, the L_a:L_s scaling relationship is stronger in relatively larger deltas (Fig. 1c). Additionally, wave-dominated deltas as defined by Nienhuis et al. (2020), also show a consistent L_a:L_s relationship. Note that some calculated backwater lengths in this study vary from, but lie within the same order of magnitude, as backwater lengths previously reported for the same sites (Chatanantavet et al., 2012; Ganti et al., 2016). This calculation difference is due to using different representative channel widths to calculate the characteristic flow depth. We used the

This article is protected by copyright. All rights reserved.

Accepted Article

channel width at the avulsion node (W_{av}), while the choice of channel width is not always explicitly stated in previous studies.

All power law relationships in Figure 1 are statistically significant. However, the relationship between the avulsion and slope break length for the global dataset has the strongest correlation (Fig. 1c; R^2 = 63%, RMSE = 0.36). Of the studied deltas (n = 80), 65% lie within the 95% confidence interval of the regression line (Fig. 1c) in comparison to Fig. 1a and 1b (64% and 55%, respectively). L_a and L_s are related with exponent 1, showing a direct scaling relationship.

We also classified the L_a:L_s relationship (Fig. 1c) by valley type to test whether this scaling remains consistent for all valley types. Regression slopes from alluvial, bedrock and Pleistocene valley types are not significantly different from the full data set although valley-confined deltas do show a difference. The p-values shown next to regression lines (Fig. 2) are all >0.05, and the dashed lines in Fig. 2 lie within 95% confidence bands for the overall relationships (Fig. 2a-c). Valley-confined deltas are not significantly different (p-value = 0.06) from the proposed L_a:L_s from the full data set, but the regression line for this valley type deviates from our proposed L_a:L_s relationship (dashed line in Fig. 2d). The small (N=5) number of valley-confined deltas prevents interpretation of the significance of this result (Fig. 2d). Appreciable scatter is observed (1 order of magnitude of the avulsion length; range of residuals = ±0.2 in log units) in the alluvial valley deltas (Fig. 2a). Relatively small deltas also contribute to the scatter for bedrock valley types (Fig. 2b). However, the strong and relatively consistent L_a:L_s correlation across different valley types provokes consideration of the importance of this scaling relationship in the context of the previously known L_a-L_b relationship and valley-exit control on delta apex position (Ganti et al., 2016; Hartley et al., 2017).

Accepted Article

This article is protected by copyright. All rights reserved.

Accepted Article

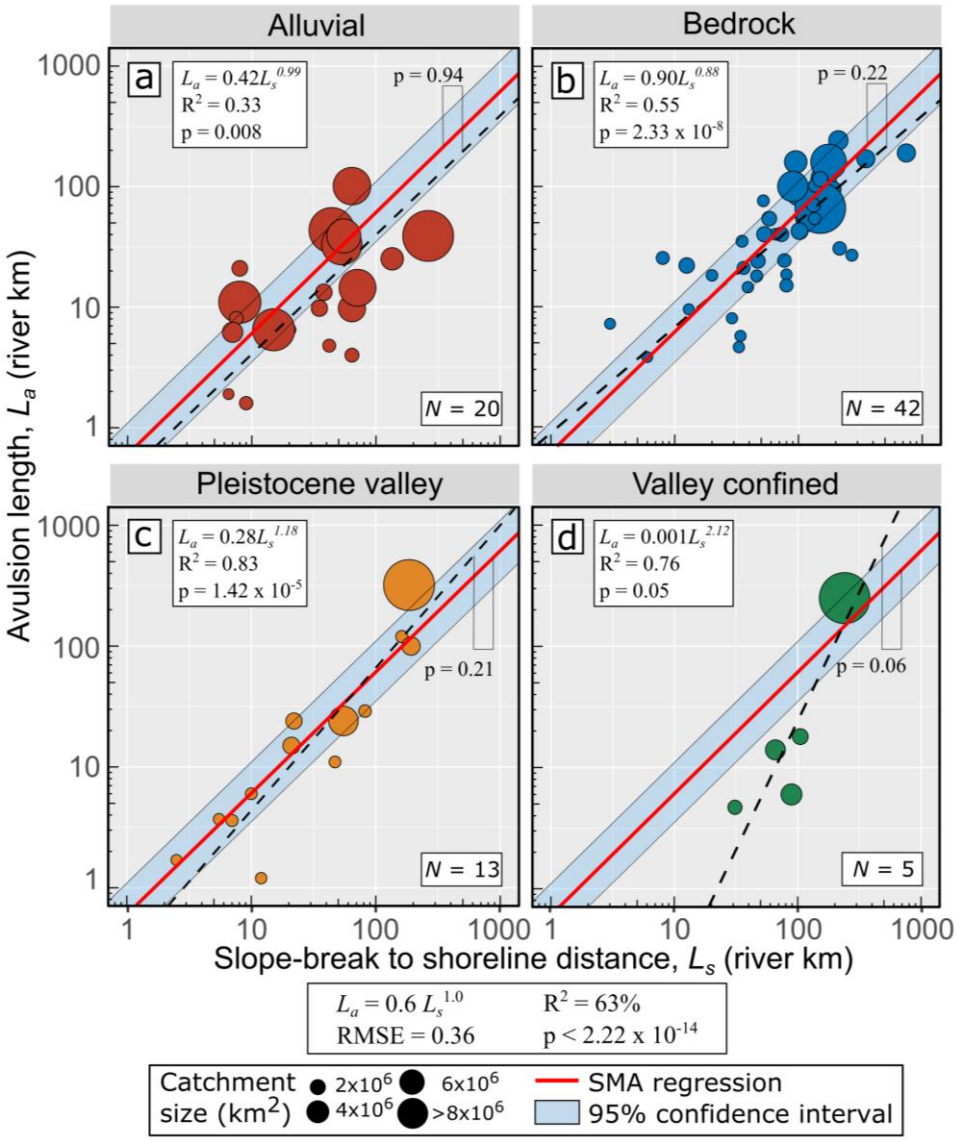

Figure 2. (a-d) Data from Fig. 1c (avulsion length (L_a) against slope break distance from the shoreline (L_s)) for each valley type. Red lines are the SMA regression lines from the full data set, dashed lines are separate SMA regression lines from each valley type with L_a-L_s relationships shown on panel. Point size is scaled with the catchment area and p-values near the regression lines are the significance of the difference between the gradient from L_a-L_s SMA regression for each valley type versus the L_a-L_s SMA regression from the full data set (i.e. slope test).

4 Discussion

Morphometric scaling and delta morphology

We demonstrate here how the calculated morphometric scaling relates to scaling on some modern deltas. Examples from the Rufiji, Ebro, Orinoco and Volga deltas show the locations of the morphometric boundaries and how the scaling between the avulsion and slope break lengths

This article is protected by copyright. All rights reserved.

measured from the shoreline is consistent across a range of delta sizes (Fig. 3a-d). Visual observation from satellite images shows that the apices of each of these deltas coincide with measured avulsion lengths (yellow points in Fig. 3a-d). As for most other deltas in the dataset, these four examples have developed in approximately their current locations since the early Holocene due to the decreasing rate of sea-level rise. Detailed studies of their avulsion histories (Aslan et al., 2003; Kroonenberg et al., 1997; Nienhuis et al., 2017) suggest that the avulsion nodes have remained in a constant locations as these deltas have developed. The avulsion-slope break length scaling ratios in these deltas are $L_a \sim 0.6L_s$ for the Rufiji delta and $L_a \sim 0.5L_s$ for the Ebro, Orinoco and Volga deltas. However, the calculated backwater lengths (L_b) from the Rufiji and Ebro deltas are located farther downstream of the avulsion nodes (white points in Fig. 3a,b,d). Both the Rufiji and Ebro deltas have $L_a \sim 1.2L_b$ instead of $L_a \sim 0.5L_b$ (or $L_a{:}L_b \sim 1{:}2$) as previously suggested by Chatanantavet et al. (2012), Ganti et al. (2016) and Jerolmack & Swenson (2007) due to the effects of using different representative channel widths to calculate backwater lengths. The Orinoco delta, however, has a calculated backwater length of 585 km that lies upstream of the delta in the river, outside of the mapped area (i.e. $L_a \sim 0.3L_b$). The Volga delta backwater length of 184 km, hence $L_a \sim 0.5L_b$, coincides with the location of the slope break ($L_s{:}L_b \sim 1{:}1$). These examples from natural deltas are consistent with our overall finding that $L_a \sim 0.6L_s$.

Accepted Article

This article is protected by copyright. All rights reserved.

Accepted Article

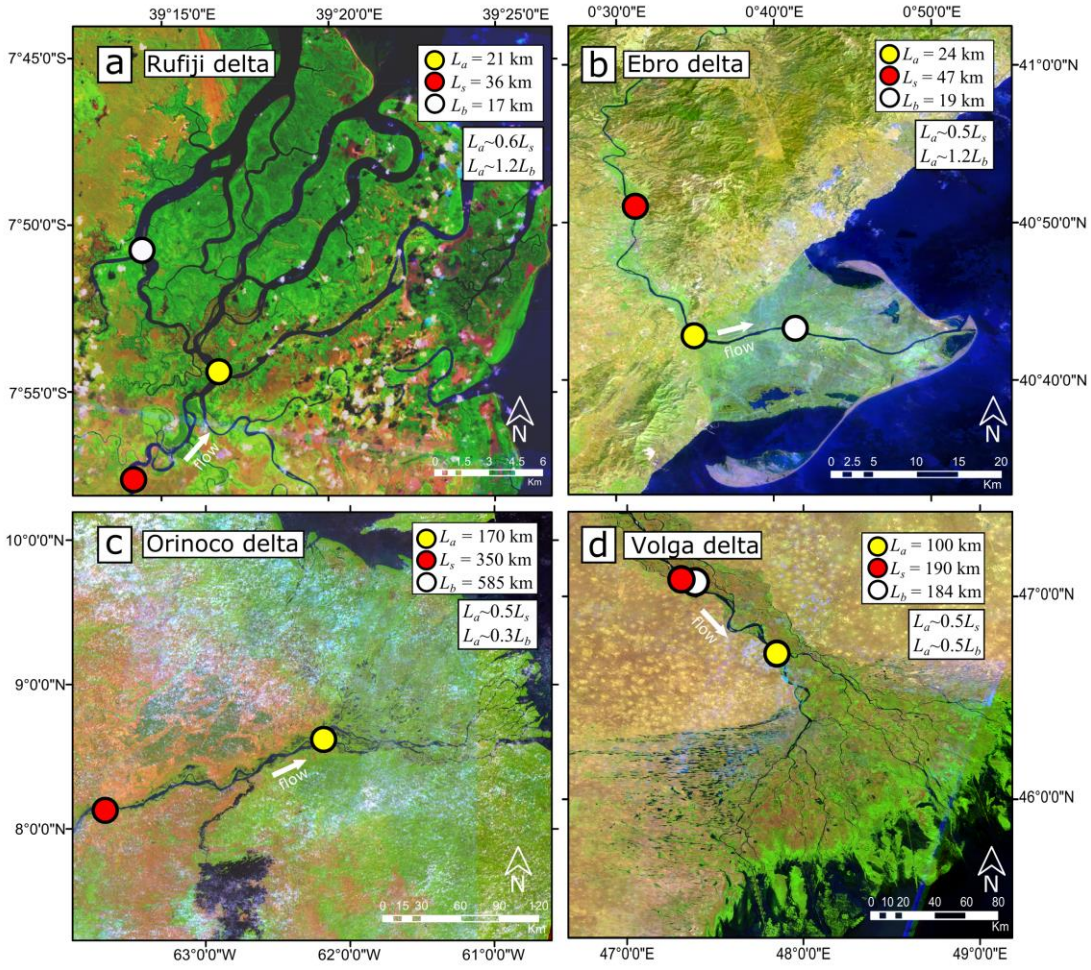

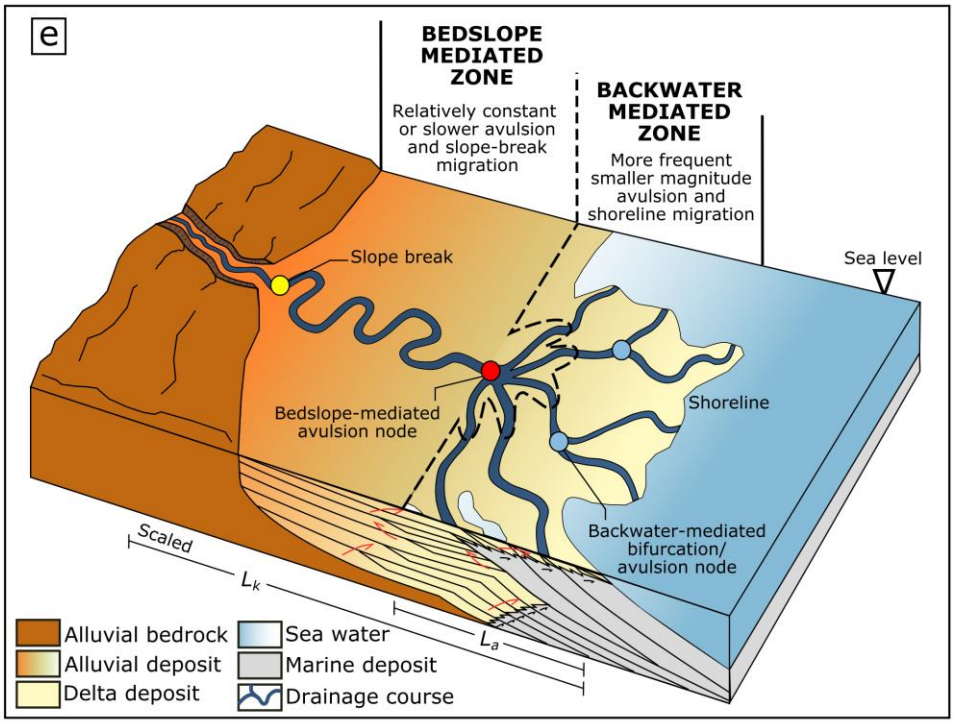

This article is protected by copyright. All rights reserved.

Figure 3. Stitched composite Landsat 5 images from year 2000 from Rufiji (a), Ebro (b) and Volga (d) deltas. The Orinoco (c) used tiled composite Landsat 7 images due to unavailability of complete near cloud-free coverage of the delta plain from Landsat 5. (e) Depositional model for deltas with bedslope- and backwater-mediated zonation. See Fig. S1a for the location of these deltas. The Near-Infrared Band 5 and 4 (1.55 - 1.75 μm and 0.76 - 0.90 μm) and Visible Band 1 (0.45 - 0.52 μm) are shown to better distinguish water and land (Text S1). Values of measured avulsion (L_a) and slope break (L_s) lengths are plotted as yellow and red points, respectively. The calculated backwater lengths (L_b) are plotted as white points; the backwater location for Fig. 3c lies outside the area shown. For Fig. 3e, the red thick arrows are the sequence packages and smaller black arrows show the smaller parasequence packages.

Processes involved in the proposed scaling relationship

Mouth-bar deposition should dominate the most distal part of a delta due to input sediment being deposited in a relatively static water body (Olariu & Bhattacharya, 2006). Upstream parts of deltas will be dominated by partial avulsion or crevasse bifurcation (Kleinhans et al., 2013), or by avulsion by incision (Slingerland & Smith, 2004) induced by in-channel aggradation due to the slope break and/or the backwater effect (Kleinhans et al., 2013; Slingerland & Smith, 2004). As shown in this study, the stronger global L_a-L_s scaling relationship suggests that the slope break is the predominant driver of channel response in the upstream part of a delta, rather than the backwater effect (L_a-L_b relationship). In-channel aggradation could then trigger avulsion in the upstream region of a delta, maintaining the scaling relationship between L_a and L_s. Hence the avulsion nodes, the most upstream bifurcation nodes of deltas, are proposed to be related to the process of in-channel aggradation due to the change in slope and may not be directly related to bifurcation or backwater processes downstream. A study from the Huanghe (Yellow) River delta showed avulsion related to a slope break (bedslope-mediated) ~700 km upstream from the shoreline, that also coincides with the valley exit from the Loess plateau, while backwater-influenced avulsions are clustered downstream near the shoreline (Ganti et al., 2014). Thus, we divide the delta development domain into upstream and downstream zones with different processes dominating in each of these two areas (Fig. 3e). Note that the upstream and downstream process domains are not necessarily sequential and may operate over different timescales. Controls over the timing and thresholds of avulsion-bifurcation cycles remain to be explored further.

The controls on slope breaks in delta channels also remain an area for further investigation. Valley-exit and alluvial-bedrock transitions, as seen from the DEMs used in this study, may control the slope break location with 1:1 L_s-L_v scaling (Fig. 1b). However, the location of the slope break is also controlled by a range of interacting factors including grain size transitions and associated changes in Shields' stress, geological controls (e.g. subsidence and lithology), and the nature of the overbank material (e.g. cohesive vs non-cohesive).

Correlation with the valley types

Fig. 2a-d show the overall scaling relationship across different valley types, but Fig. 2d shows how deltas located in valley-confined settings may depart from our calculated $L_a \sim 0.6L_s$ scaling relationship. Valley-confined deltas have limited lateral space. When in-channel aggradation triggers an avulsion, there is a higher possibility that a newly avulsed channel will rejoin the parent channel due to this limited lateral space, limiting the chance of the growth of

This article is protected by copyright. All rights reserved.

Accepted Article

distributary channels by delta plain progradation (Slingerland & Smith, 2004). Thus, our L_a-L_s scaling relationship does not fit in this valley type (Fig. 2d). As an example, the Paraná delta (Argentina) is valley confined from the hinterland all the way to the shoreline which confines the lateral growth of the delta as seen in its DEM (Fig. S8). Additionally, alluvial valleys that are under the influence of erosion instead of prograding or aggrading may contribute to the scattered data in Fig. 2a. These observations enhance our understanding that the valley exit does not necessarily coincide with the slope break, but that valley exit is coincident with the avulsion node only in certain valley types (Hartley et al., 2017).

Implication of the proposed scaling relationship

From the close relationship between the slope break length and the avulsion length, we propose an updated conceptual model of delta lobe building (Fig. 3e). We divide deltas into bedslope-mediated and backwater-mediated zones, as proposed by Ganti et al. (2014) from their Huanghe (Yellow) delta case study. The bedslope-mediated zone includes the upstream catchment area and fluvial environments as far downstream as the first avulsion point, initiating the onset of delta construction and generation of avulsion-driven stratigraphy. The backwater-mediated zone consists of delta distributary channels down to the shoreline. In the bedslope-mediated zone, the slope break and avulsion lengths (shown in distal stratigraphy, and red and yellow circle symbols on the delta plain in Fig. 3e) will migrate over long (~10-100 ka) avulsion timescales, depending on the size of the delta involved. In the backwater-mediated zone, bifurcation nodes and shorelines will be more sensitive to allogenic forcing (sea-level fluctuation, subsidence) and thus they may migrate more frequently (i.e. ~10^1-10^3 years) at smaller magnitudes (shown in the proximal stratigraphy and light blue circle symbols on the delta plain in Fig. 3e). Different response times are due to different compensation scale and different channel depths and aggradation rates between the upstream and downstream parts of a delta (Jerolmack & Paola, 2010; Li et al., 2018; Li et al., 2016; Straub et al., 2020). Transgressive and regressive parasequences may be recorded in the stratigraphy of the backwater-mediated zone in a more serrated manner (stratigraphy shown in Fig. 3e), whereas in the upstream part, the smaller allogenic forcing may be shredded due to longer timescales involved in the bedslope-mediated zone (Li et al., 2018). These differences imply that the distal zone will have more frequent shoreline and bifurcation node migration compared to the proximal area. Thus, changes in sea-level or subsidence may cause migration of the backwater-mediated avulsion nodes, but the bedslope-mediated avulsion node will remain constant due to its connection with aggradation at the slope break.

This conceptual model is corroborated by recent numerical modelling (Ratliff et al., 2021) which demonstrated the interconnection between avulsion and the slope break length. They proposed that the location of the avulsion node always occurs at the slope break due to the linear diffusion of aggradation and erosion of the river profile. Under sea-level rise, the slope break and avulsion lengths (in the form of backwater length) will remain constant under varying magnitudes of sea-level rise rate (*SLRR*), consistent with our conceptual model (Fig. 3e; their Fig. 2a and 2b). Our data set also includes 10 wave-dominated deltas that follow the same L_a-L_s scaling relationship as the river-dominated deltas in our study. The Ratliff et al (2021) study shows the consistency of this L_a-L_s geometric constraint across different wave energies (their Fig. 2b). Nonetheless, upstream retreat of the avulsion node and slope break may happen under sea-level rise (their Fig. 1d). Even so, the L_a-L_s (avulsion and slope break length) scaling remains constant even under sea-level rise, supporting our conceptual model (Fig. 3e).

This article is protected by copyright. All rights reserved.

Accepted Article

Scatter in the dataset

Most modern global deltas have developed since the early Holocene, associated with a decreasing eustatic sea-level rise rate, during which there have been natural and anthropogenic changes of boundary conditions (e.g. sediment supply, water discharge, sea-level rise) (Bird et al., 2010; Ericson et al., 2006; Stanley & Warne, 1994). The data that we derived from satellite imagery represent snapshots of delta response to these cumulative interacting boundary conditions. Although some measured individual delta morphologies may be transient responses to changing boundary conditions, we assume that the overall data set represents deltas in dynamic equilibrium with the environmental controls (Mackin, 1948). However, some of the scatter in Figure 1 may be attributed to transient responses to, for example, reductions in river flow and sediment input (Li et al., 2017) or sea-level rise (Nienhuis & van de Wal, 2021).

The relative age of a delta should also impact its L_a:L_s scaling. Adopting the theoretical approach to delta distributary networks from Jerolmack & Swenson (2007), delta building by bifurcation-dominated processes will occur early in delta development. As bifurcation continues, a landward-shift in aggradation or channel backfilling will trigger avulsion by deposition in upstream reaches, previously known as backwater length-controlled (Edmonds et al., 2009; Slingerland & Smith, 2004). Thus, it is proposed that older (or larger) deltas will be avulsion-dominated or bedslope-mediated instead of bifurcation-dominated, where the change in surface water slope induces a decrease in sediment transport capacity, triggering bedslope-mediated avulsion (Ganti et al., 2016). Similarly, it is proposed that small, or relatively younger, deltas tend to be characterized by bifurcation-dominated processes, and therefore may depart from the overall L_a:L_s scaling relationship (Fig. 1c).

The Po, Mississippi and Mekong deltas demonstrate how engineering work may disrupt the dynamic equilibrium assumption that underpins the proposed scaling relationships. The Po delta has experienced extensive hydraulic works over several centuries, including the 'Porto Viro' bypass in 1604, dredging, beach reclamation, channel bank protection, and subsidence due to groundwater extraction (Ninfo et al., 2018). Channel bypassing directly influenced the delta avulsion length that makes the $L_a \sim 0.6L_s$ scaling relationship overestimate the present day avulsion length by a factor of 4 (i.e. $L_a \sim 0.15L_s$) (Fig. 1c). Anthropogenic modification is also evident on the Mississippi delta. Artificial cutoff in 1831 minimized the flow coming into the human-made Atchafalaya delta complex, but then dredging in 1880 in the Old River area maintained the flow to both Atchafalaya and Balize delta complexes. The $L_a \sim 0.6L_s$ scaling relationship that we calculate underestimates the modern avulsion node in the Mississippi delta that is consistently located at Old River (~320 km from the recent shoreline; $L_a \sim 1.7L_s$) (Fig. 1c) (Aslan et al., 2005). Detailed study of Mekong delta morphodynamics has also shown how sediment starvation and dam construction is significantly decreasing the delta progradation rate (Li et al., 2017). This human-made modification causes our scaling relationship to underestimate the present day avulsion length (i.e. $L_a \sim 1.7L_s$) (Fig. 1c). Hence, century-scale engineering can affect the proposed scaling relationship even in large deltas.

Data quality also contributes to the uncertainty of the $L_a \sim 0.6L_s$ scaling relationship. For smaller deltas that have relatively short avulsion lengths (e.g. the Comal delta; La = 4 km) shows uncertainty in extracting the slope break location from the elevation profile, in contrast to the larger (La = 160 km) Nile delta (Fig. S4a-c and Fig. S4d-f). Common gross error shown in the ArcticDEM dataset also contributes to the difficulty in defining the exact location of a slope break from the elevation profile (Błaszczyk et al., 2019).

This article is protected by copyright. All rights reserved.

Accepted Article

5 Conclusions

A sample of 105 global deltas provides a comprehensive assessment of delta morphometric scaling relationships. We show that the avulsion-backwater length scaling relationship is less consistent in this global dataset than previously proposed. The results also show that the valley exit does not necessarily coincide with a break in slope but rather with the avulsion node in certain valley types. Further to these scaling relationships, we show that the avulsion length scales most consistently and most strongly with the slope break length, followed by the valley-exit-to-shoreline distance. These findings open the opportunity to explore alternative hypotheses for the controls over delta development. Along with the possible processes that produce these scaling relationships, we propose a framework for understanding delta lobe building by dividing a delta into bedslope- and backwater-mediated zones. The proposed framework allows potential insights into how delta systems will respond to changing boundary conditions. This framework also contributes to our understanding of the location and frequency of avulsion nodes in a delta system that is fundamental for the large populations that live on the world's delta plains.

Acknowledgments

This research was funded by an Indonesia Endowment Fund for Education (LPDP) award to Prasojo.

Open Research

The global river discharge dataset is available from The Global Runoff Data Centre (GRDC), 56068 Koblenz, Germany and via the web (https://www.bafg.de/GRDC/EN/02_srvcs/21_tmsrs/210_prtl/prtl_node.html). The dataset used in this study (Table S1) is available at https://doi.org/10.6084/m9.figshare.16429998.v1.

References

Aiken, S. J., & Brierley, G. J. (2013). Analysis of longitudinal profiles along the eastern margin of the Qinghai-Tibetan Plateau. *Journal of Mountain Science*, *10*(4), 643–657. https://doi.org/10.1007/s11629-013-2814-2

Aslan, A., Autin, W. J., & Blum, M. D. (2005). Causes of river avulsion: Insights from the late Holocene avulsion history of the Mississippi River, U.S.A. *Journal of Sedimentary Research*, *75*(4), 650–664. https://doi.org/10.2110/jsr.2005.053

Aslan, A., White, W. A., Warne, A. G., & Guevara, E. H. (2003). Holocene evolution of the western Orinoco Delta, Venezuela. *GSA Bulletin*, *115*(4), 479–498. Retrieved from http://pubs.geoscienceworld.org/gsa/gsabulletin/article-pdf/115/4/479/3389566/i0016-7606-115-4-479.pdf

Beck, H. E., Zimmermann, N. E., McVicar, T. R., Vergopolan, N., Berg, A., & Wood, E. F. (2018). Present and future köppen-geiger climate classification maps at 1-km resolution. *Scientific Data*, *5*(1), 1–12. https://doi.org/10.1038/sdata.2018.214

Besset, M., Anthony, E. J., & Bouchette, F. (2019). Multi-decadal variations in delta shorelines and their relationship to river sediment supply: An assessment and review. *Earth-Science Reviews*, Vol. 193, pp. 199–219. https://doi.org/10.1016/j.earscirev.2019.04.018

Besset, M., Anthony, E. J., & Sabatier, F. (2017). River delta shoreline reworking and erosion in the Mediterranean and Black Seas: the potential roles of fluvial sediment starvation and

This article is protected by copyright. All rights reserved.

other factors. *Elem Sci Anth*, *5*(0), 54. https://doi.org/10.1525/elementa.139
Bird, M. I., Austin, W. E. N., Wurster, C. M., Fifield, L. K., Mojtahid, M., & Sargeant, C. (2010). Punctuated eustatic sea-level rise in the early mid-Holocene. *Geology*, *38*(9), 803–806. https://doi.org/10.1130/G31066.1
Bishop, P., Hoey, T. B., Jansen, J. D., & Lexartza Artza, I. (2005). Knickpoint recession rate and catchment area: The case of uplifted rivers in Eastern Scotland. Earth Surface Processes and Landforms, 30(6), 767–778. https://doi.org/10.1002/esp.1191
Błaszczyk, M., Ignatiuk, D., Grabiec, M., Kolondra, L., Laska, M., Decaux, L., et al. (2019). Quality assessment and glaciological applications of digital elevation models derived from space-borne and aerial images over two tidewater glaciers of southern spitsbergen. *Remote Sensing*, *11*(9), 1121. https://doi.org/10.3390/rs11091121
Brooke, S. A. S., Ganti, V., Chadwick, A. J., & Lamb, M. P. (2020). Flood Variability Determines the Location of Lobe- Scale Avulsions on Deltas: Madagascar. *Geophysical Research Letters*, *47*(20), e2020GL088797. https://doi.org/10.1029/2020GL088797
Burgers, H. E. R., Schipper, A. M., & Jan Hendriks, A. (2014). Size relationships of water discharge in rivers: scaling of discharge with catchment area, main-stem length and precipitation. Hydrological Processes, 28(23), 5769–5775. https://doi.org/10.1002/hyp.10087
Caldwell, R. L., Edmonds, D. A., Baumgardner, S., Paola, C., Roy, S., & Nienhuis, J. H. (2019). A global delta dataset and the environmental variables that predict delta formation on marine coastlines. *Earth Surface Dynamics*, *7*(3), 773–787. https://doi.org/10.5194/esurf-7-773-2019
Chadwick, A. J., Lamb, M. P., Moodie, A. J., Parker, G., & Nittrouer, J. A. (2019). Origin of a Preferential Avulsion Node on Lowland River Deltas. *Geophysical Research Letters*, *46*(8), 4267–4277. https://doi.org/10.1029/2019GL082491
Chatanantavet, P., Lamb, M. P., & Nittrouer, J. A. (2012). Backwater controls of avulsion location on deltas. *Geophysical Research Letters*, *39*(1), 2–7. https://doi.org/10.1029/2011GL050197
Cleveland, W. S. (1979). Robust locally weighted regression and smoothing scatterplots. Journal of the American Statistical Association, 74(368), 829–836. https://doi.org/10.1080/01621459.1979.10481038
Correggiari, A., Cattaneo, A., & Trincardi, F. (2005). Depositional Patterns in The Late Holocene Po Delta System. *SEPM Special Publication*, (83), 365–392. Retrieved from http://radiocarbon.pa.qub.ac.uk/marine/
Edmonds, D. A., & Slingerland, R. L. (2008). Stability of delta distributary networks and their bifurcations. *Water Resources Research*, *44*(9). https://doi.org/10.1029/2008WR006992
Edmonds, Douglas A., Hoyal, D. C. J. D., Sheets, B. A., & Slingerland, R. L. (2009). Predicting delta avulsions: Implications for coastal wetland restoration. *Geology*, *37*(8), 759–762. https://doi.org/10.1130/G25743A.1
Ericson, J. P., Vörösmarty, C. J., Dingman, S. L., Ward, L. G., & Meybeck, M. (2006). Effective sea-level rise and deltas: Causes of change and human dimension implications. *Global and Planetary Change*, *50*(1–2), 63–82. https://doi.org/10.1016/j.gloplacha.2005.07.004
Farr, T. G., Rosen, P. A., Caro, E., Crippen, R., Duren, R., Hensley, S., et al. (2007). The shuttle radar topography mission. *Reviews of Geophysics*, *45*(2). https://doi.org/10.1029/2005RG000183
Fernandes, A. M., Törnqvist, T. E., Straub, K. M., & Mohrig, D. (2016). Connecting the

This article is protected by copyright. All rights reserved.

backwater hydraulics of coastal rivers to fluviodeltaic sedimentology and stratigraphy. *Geology*, *44*(12), 979–982. https://doi.org/10.1130/G37965.1

Gailleton, B., Mudd, S. M., Clubb, F. J., Peifer, D., & Hurst, M. D. (2019). A segmentation approach for the reproducible extraction and quantification of knickpoints from river long profiles. Earth Surface Dynamics, 7(1), 211–230. https://doi.org/10.5194/esurf-7-211-2019

Ganti, V., Chadwick, A. J., Hassenruck-Gudipati, H. J., Fuller, B. M., & Lamb, M. P. (2016). Experimental river delta size set by multiple floods and backwater hydrodynamics. *Science Advances*, *2*(5), e1501768. https://doi.org/10.1126/sciadv.1501768

Ganti, V., Chu, Z., Lamb, M. P., Nittrouer, J. A., & Parker, G. (2014). Testing morphodynamic controls on the location and frequency of river avulsions on fans versus deltas: Huanghe (Yellow River), China. *Geophysical Research Letters*, *41*(22), 7882–7890. https://doi.org/10.1002/2014GL061918

Ganti, V., Lamb, M. P., & Chadwick, A. J. (2019). Autogenic Erosional Surfaces in Fluvio-deltaic Stratigraphy from Floods, Avulsions, and Backwater Hydrodynamics. *Journal of Sedimentary Research*, *89*(8), 815–832. https://doi.org/10.2110/jsr.2019.40

Gorelick, N., Hancher, M., Dixon, M., Ilyushchenko, S., Thau, D., & Moore, R. (2017). Google Earth Engine: Planetary-scale geospatial analysis for everyone. Remote Sensing of Environment, 202, 18–27. https://doi.org/10.1016/j.rse.2017.06.031

Hack, J. T. (1973). Stream-profile analysis and stream-gradient index. Journal of Research of the U.S. Geological Survey, 1(4), 421–429.

Hartley, A. J., Weissmann, G. S., & Scuderi, L. (2017). Controls on the apex location of large deltas. *Journal of the Geological Society*, *174*(1), 10–13. https://doi.org/10.1144/jgs2015-154

Hayakawa, Y. S., & Oguchi, T. (2006). DEM-based identification of fluvial knickzones and its application to Japanese mountain rivers. *Geomorphology*, *78*(1–2), 90–106. https://doi.org/10.1016/j.geomorph.2006.01.018

Hoitink, A. J. F., Wang, Z. B., Vermeulen, B., Huismans, Y., & Kästner, K. (2017). Tidal controls on river delta morphology. *Nature Geoscience*, *10*(9), 637–645. https://doi.org/10.1038/ngeo3000

Jerolmack, D. J., & Mohrig, D. (2007). Conditions for branching in depositional rives. *Geology*, *35*(5), 463–466. https://doi.org/10.1130/G23308A.1

Jerolmack, D. J., & Paola, C. (2010). Shredding of environmental signals by sediment transport. *Geophysical Research Letters*, *37*(19). https://doi.org/10.1029/2010GL044638

Jerolmack, D. J., & Swenson, J. B. (2007). Scaling relationships and evolution of distributary networks on wave-influenced deltas. *Geophysical Research Letters*, *34*(23), n/a-n/a. https://doi.org/10.1029/2007GL031823

Kirby, E., & Whipple, K. X. (2012). Expression of active tectonics in erosional landscapes. Journal of Structural Geology, 44, 54–75. https://doi.org/10.1016/j.jsg.2012.07.009

Kleinhans, M. G., Ferguson, R. I., Lane, S. N., & Hardy, R. J. (2013). Splitting rivers at their seams: bifurcations and avulsion. *Earth Surface Processes and Landforms*, *38*(1), 47–61. https://doi.org/10.1002/esp.3268

Kroonenberg, S. B., Rusakov, G. V., & Svitoch, A. A. (1997). The wandering of the Volga delta: A response to rapid Caspian sea-level change. *Sedimentary Geology*, *107*(3–4), 189–209. https://doi.org/10.1016/S0037-0738(96)00028-0

Lehner, B., & Grill, G. (2013). Global river hydrography and network routing: Baseline data and new approaches to study the world's large river systems. *Hydrological Processes*, *27*(15),

This article is protected by copyright. All rights reserved.

2171–2186. https://doi.org/10.1002/hyp.9740
Li, Q., Gasparini, N. M., & Straub, K. M. (2018). Some signals are not the same as they appear: How do erosional landscapes transform tectonic history into sediment flux records? *Geology*, *46*(5), 407–410. https://doi.org/10.1130/G40026.1
Li, Q., Yu, L., & Straub, K. M. (2016). Storage thresholds for relative sea-level signals in the stratigraphic record. *Geology*, *44*(3), 179–182. https://doi.org/10.1130/G37484.1
Li, X., Liu, J. P., Saito, Y., & Nguyen, V. L. (2017). Recent evolution of the Mekong Delta and the impacts of dams. *Earth-Science Reviews*, *175*(March), 1–17. https://doi.org/10.1016/j.earscirev.2017.10.008
Mackin, J. H. (1948). Concept of the graded river. *Bulletin of The Geological Society of America*, *59*, 463–512.
Milly, P. C. D., Dunne, K. A., & Vecchia, A. V. (2005). Global pattern of trends in streamflow and water availability in a changing climate. Nature, 438(7066), 347–350. https://doi.org/10.1038/nature04312
Morin, P., Porter, C., Cloutier, M., Howat, I., Noh, M.-J., Willis, M., et al. (2016). ArcticDEM; A Publically Available, High Resolution Elevation Model of the Arctic. In *Geophysical Research Abstracts* (Vol. 18). Retrieved from https://ui.adsabs.harvard.edu/abs/2016EGUGA..18.8396M/abstract
Mueller, E. R., Schmidt, J. C., Topping, D. J., Shafroth, P. B., Rodríguez-Burgueño, J. E., Ramírez-Hernández, J., et al. (2017). Geomorphic change and sediment transport during a small artificial flood in a transformed post-dam delta: The Colorado River delta, United States and Mexico. *Ecological Engineering*, *106*, 757–775. https://doi.org/10.1016/j.ecoleng.2016.08.009
Nienhuis, J. H., Ashton, A. D., Edmonds, D. A., Hoitink, A. J. F., Kettner, A. J., Rowland, J. C., et al. (2020). Global-scale human impact on delta morphology has led to net land area gain. *Nature*, *577*(7791), 514–518. https://doi.org/10.1038/s41586-019-1905-9
Nienhuis, J. H., & van de Wal, R. S. W. (2021). Projections of Global Delta Land Loss From Sea-Level Rise in the 21st Century. *Geophysical Research Letters*, *48*(14), e2021GL093368. https://doi.org/10.1029/2021GL093368
Nienhuis, Jaap H., Ashton, A. D., Kettner, A. J., & Giosan, L. (2017). Large-scale coastal and fluvial models constrain the late Holocene evolution of the Ebro Delta. *Earth Surface Dynamics*, *5*(3), 585–603. https://doi.org/10.5194/esurf-5-585-2017
Nijhuis, A. G., Edmonds, D. A., Caldwell, R. L., Cederberg, J. A., Slingerland, R. L., Best, J. L., et al. (2015). Fluvio-deltaic avulsions during relative sea-level fall. *Geology*, *43*(8), 719–722. https://doi.org/10.1130/G36788.1
Ninfo, A., Ciavola, P., & Billi, P. (2018). The Po Delta is restarting progradation: Geomorphological evolution based on a 47-years Earth Observation dataset. *Scientific Reports*, *8*(1). https://doi.org/10.1038/s41598-018-21928-3
Olariu, C., & Bhattacharya, J. P. (2006). Terminal distributary channels and delta front architecture of river-dominated delta systems. *Journal of Sedimentary Research*, *76*(2), 212–233. https://doi.org/10.2110/jsr.2006.026
Paola, C., & Mohrig, D. (1996). Palaeohydraulics revisited: Palaeoslope estimation in coarse-grained braided rivers. In *Basin Research* (Vol. 8). https://doi.org/10.1046/j.1365-2117.1996.00253.x
Parker, G., Wilcock, P. R., Paola, C., Dietrich, W. E., & Pitlick, J. (2007). Physical basis for quasi-universal relations describing bankfull hydraulic geometry of single-thread gravel bed

This article is protected by copyright. All rights reserved.

rivers. *Journal of Geophysical Research: Earth Surface*, *112*(4). https://doi.org/10.1029/2006JF000549

Pritchard, D., Roberts, G. G., White, N. J., & Richardson, C. N. (2009). Uplift histories from river profiles. Geophysical Research Letters, 36(24), L24301. https://doi.org/10.1029/2009GL040928

Ratliff, K. M., Hutton, E. W. H., & Murray, A. B. (2021). Modeling long-term delta dynamics reveals persistent geometric river avulsion locations. *Earth and Planetary Science Letters*, *559*, 116786. https://doi.org/10.1016/j.epsl.2021.116786

Rodríguez, E., Morris, C. S., & Eric Belz, J. (2006). A Global Assessment of the SRTM Performance. In Photogrammetric Engineering & Remote Sensing (Vol. 72). Retrieved from http://gipsy.jpl.nasa.gov

Slingerland, R., & Smith, N. D. (2004). River Avulsions and Their Deposits. *Annual Review of Earth and Planetary Sciences*, *32*(1), 257–285. https://doi.org/10.1146/annurev.earth.32.101802.120201

Stanley, D. J., & Warne, A. G. (1994). Worldwide initiation of Holocene marine deltas by deceleration of sea-level rise. *Science*, *265*(5169), 228–231. https://doi.org/10.1126/science.265.5169.228

Straub, K. M., Duller, R. A., Foreman, B. Z., & Hajek, E. A. (2020). Buffered, Incomplete, and Shredded: The Challenges of Reading an Imperfect Stratigraphic Record. *Journal of Geophysical Research: Earth Surface*, *125*(3), e2019JF005079. https://doi.org/10.1029/2019JF005079

Syvitski, J. P. M., Kettner, A. J., Overeem, I., Hutton, E. W. H., Hannon, M. T., Brakenridge, G. R., et al. (2009). Sinking deltas due to human activities. *Nature Geoscience*, *2*(10), 681–686. https://doi.org/10.1038/ngeo629

Syvitski, J. P. M., & Saito, Y. (2007). Morphodynamics of deltas under the influence of humans. *Global and Planetary Change*, *57*(3–4), 261–282. https://doi.org/10.1016/j.gloplacha.2006.12.001

Ta, T. K. O., Nguyen, V. L., Tateishi, M., Kobayashi, I., Saito, Y., & Nakamura, T. (2002). Sediment facies and Late Holocene progradation of the Mekong River Delta in Bentre Province, southern Vietnam: An example of evolution from a tide-dominated to a tide- and wave-dominated delta. *Sedimentary Geology*, *152*(3–4), 313–325. https://doi.org/10.1016/S0037-0738(02)00098-2

Tessler, Z. D., Vörösmarty, C. J., Grossberg, M., Gladkova, I., Aizenman, H., Syvitski, J. P. M., et al. (2015). Profiling risk and sustainability in coastal deltas of the world. *Science*, *349*(6248), 638–643. https://doi.org/10.1126/science.aab3574

Tucker, C. J., Grant, D. M., & Dykstra, J. D. (2004). NASA's global orthorectified landsat data set. *Photogrammetric Engineering and Remote Sensing*, *70*(3), 313–322. https://doi.org/10.14358/PERS.70.3.313

Wang, H., Wu, X., Bi, N., Li, S., Yuan, P., Wang, A., et al. (2017). Impacts of the dam-orientated water-sediment regulation scheme on the lower reaches and delta of the Yellow River (Huanghe): A review. *Global and Planetary Change*, Vol. 157, pp. 93–113. https://doi.org/10.1016/j.gloplacha.2017.08.005

Warrick, J. A., Stevens, A. W., Miller, I. M., Harrison, S. R., Ritchie, A. C., & Gelfenbaum, G. (2019). World's largest dam removal reverses coastal erosion. *Scientific Reports*, *9*(1), 1–12. https://doi.org/10.1038/s41598-019-50387-7

Willett, S. D., & Brandon, M. T. (2002). On steady states in mountain belts. Geology, 3(2), 175.

This article is protected by copyright. All rights reserved.

Retrieved from https://pubs.geoscienceworld.org/gsa/geology/article-pdf/30/2/175/3524227/i0091-7613-30-2-175.pdf

Wolman, M. G., & Miller, J. P. (1960). Magnitude and Frequency of Forces in Geomorphic Processes. *The Journal of Geology*, *68*(1), 54–74. https://doi.org/10.1086/626637

Wu, X., Bi, N., Syvitski, J., Saito, Y., Xu, J., Nittrouer, J. A., et al. (2020). Can Reservoir Regulation Along the Yellow River Be a Sustainable Way to Save a Sinking Delta? *Earth's Future*, *8*(11), e2020EF001587. https://doi.org/10.1029/2020EF001587

Yang, S. L. (2005). Impact of dams on Yangtze River sediment supply to the sea and delta intertidal wetland response. *Journal of Geophysical Research*, *110*(F3), F03006. https://doi.org/10.1029/2004JF000271

Zaprowski, B. J., Evenson, E. B., Pazzaglia, F. J., & Epstein, J. B. (2001). Knickzone propagation in the Black Hills and northern High Plains: A different perspective on the late Cenozoic exhumation of the Laramide Rocky Mountains. Geology, 29(6), 547–550. https://doi.org/10.1130/0091-7613(2001)029<0547:KPITBH>2.0.CO;2

Accepted Article

This article is protected by copyright. All rights reserved.